

Revisiting the model for radiative neutrino masses with dark matter in the $U(1)_{B-L}$ gauge theory

Shinya Kanemura,^{1,*} Yushi Mura,^{1,†} and Guohao Ying^{1,‡}

¹*Department of Physics, Osaka University, Toyonaka, Osaka 560-0043, Japan*

Abstract

The radiative seesaw model with gauged $U(1)_{B-L} \times \mathbb{Z}_2$ extension is a well-motivated scenario which gives consistent predictions of active neutrino masses and the abundance of dark matter. Majorana masses of right-handed neutrinos, the lightest of which can be identified as dark matter, are given by the spontaneous breaking of the $U(1)_{B-L}$ gauge symmetry. We revisit this model with the latest constraints from dark matter searches, neutrino oscillations, flavor experiments and collider experiments. We explore the feasible parameter space of this model, and find that there are still allowed regions under the latest experimental constraints. We present new viable benchmark scenarios for this model, i.e., the right-handed neutrino dark matter scenario and the scalar dark matter scenario. We also mention the testability of these benchmark scenarios at future experiments.

* kanemu@het.phys.sci.osaka-u.ac.jp

† y_mura@het.phys.sci.osaka-u.ac.jp

‡ ying@het.phys.sci.osaka-u.ac.jp

I. INTRODUCTION

Having the discovery of the Higgs boson at the Large Hadron Collider (LHC) in 2012, all the fundamental particles in the Standard Model (SM) of particle physics have been verified by experiments. However, there are some physics phenomena that the SM cannot explain. First, observations of the neutrino oscillation reveal that neutrinos have non-zero masses [1]. Second, the latest observation data provided by the Planck satellite [2] shows that approximately one quarter of the energy density in our universe is composed of non-baryonic and non-luminous matter, known as dark matter (DM). If the nature of dark matter is the weakly interacting massive particle (WIMP) [3, 4], the observed relic abundance can be satisfied with electroweak mass scale DM candidates. In addition, the universe exhibits matter and antimatter asymmetry.

A pioneer to explain the neutrino mass is the so-called seesaw mechanism [5–14], which generates tiny neutrino masses at tree level. For example, the type-I seesaw model [5–8] can explain tiny neutrino masses with very heavy right-handed (RH) neutrinos or very small Yukawa couplings. On the other hand, in order to explain not only tiny neutrino masses, but also dark matter simultaneously, models with radiatively generated neutrino masses [15–21] have often been studied, in which dark matter candidates are running in the loop of neutrino masses [18–21]. A representative example is the model proposed by Tao and Ma [19, 20], which can explain observed neutrino masses with TeV scale dark matter. However, this model does not explain the Majorana masses of RH neutrinos. The origin of Majorana masses of RH neutrinos can be explained in the radiative seesaw model with gauged $U(1)_{B-L} \times \mathbb{Z}_2$ extension [22]. RH neutrinos receive their masses through the spontaneous symmetry breaking (SSB) of the $U(1)_{B-L}$ gauge symmetry [23]. In Ref. [22], the observed DM relic abundance can be realized through the pair annihilation via the s -channel scalar exchange by the mixing between the SM Higgs field and the extra scalar singlet. The stability of DM, which is the lightest RH neutrino, is guaranteed by the unbroken \mathbb{Z}_2 symmetry. Tiny neutrino masses are generated radiatively via the one-loop induced operator. Some phenomenology of this model have been studied by Ref. [24, 25].

In this paper, we revisit the radiative seesaw model with gauged $U(1)_{B-L} \times \mathbb{Z}_2$ extension [22], which was originally proposed before the discovery of the Higgs boson. Since experiments have made great progress in recent years, including flavor experiments [26–30], collider experiments [31–38], neutrino oscillation measurements [39] and dark matter searches [2, 40], it would be valuable to study whether there is still allowed parameter region where tiny neutrino masses and dark matter can be explained simultaneously under current constraints. We first discuss theoretical and

| | Q^i | u_R^i | d_R^i | L^i | e_R^i | Φ | N_α | η | S |
|----------------|---------------|---------------|----------------|----------------|----------|---------------|------------|---------------|----------|
| $SU(3)_C$ | 3 | 3 | 3 | 1 | 1 | 1 | 1 | 1 | 1 |
| $SU(2)_L$ | 2 | 1 | 1 | 2 | 1 | 2 | 1 | 2 | 1 |
| $U(1)_Y$ | $\frac{1}{6}$ | $\frac{2}{3}$ | $-\frac{1}{3}$ | $-\frac{1}{2}$ | -1 | $\frac{1}{2}$ | 0 | $\frac{1}{2}$ | 0 |
| $U(1)_{B-L}$ | $\frac{1}{3}$ | $\frac{1}{3}$ | $\frac{1}{3}$ | -1 | -1 | 0 | -1 | 0 | $+2$ |
| \mathbb{Z}_2 | + | + | + | + | + | + | - | - | + |

TABLE I. Particle content and their quantum numbers.

experimental constraints on this model. We then consider neutrino masses, lepton flavor violation and DM physics in this model. We show the relic density of DM at our benchmark point. The possible parameter space under current constraints is shown. We then scan the allowed parameter space and give possible mass regions of DM. Finally, we discuss the testability of this model at future experiments, including flavor experiments, collider experiments and DM detection experiments.

This paper is organized as follows. In section II, we introduce the content of this model and give predictions of neutrino masses. In section III, we show theoretical constraints and the latest experimental constraints for this model. In section IV, we give predictions of lepton flavor violation in this model. In section V, we give the analysis of the lightest RH neutrino DM scenario and briefly discuss about the lightest inert scalar DM scenario. In section VI, we mention the testability of this model at future experiments. In section VII, we summarize this work and give our conclusions.

II. THE MODEL

The radiative seesaw model with gauged $U(1)_{B-L} \times \mathbb{Z}_2$ extension [22] is a simple extension of the SM, in which we try to explain radiative generation of neutrino masses with providing possible dark matter candidates. This model is an extension of the SM with three \mathbb{Z}_2 odd right-handed neutrinos N_α ($\alpha = 1, 2, 3$), a \mathbb{Z}_2 odd scalar $SU(2)_L$ doublet η , a scalar singlet S and an electrically neutral $U(1)_{B-L}$ gauge boson Z' . The Lagrangian is invariant under the gauge group $SU(3)_C \times SU(2)_L \times U(1)_Y \times U(1)_{B-L}$ with an unbroken \mathbb{Z}_2 discrete symmetry. The particle content is shown in Table I.

The relevant interaction \mathcal{L}_{int} for our discussion is given by

$$\mathcal{L}_{\text{int}} = \mathcal{L}_{\text{Yukawa}}^{\text{SM}} + \mathcal{L}_N - V(\Phi, \eta, S), \quad (1)$$

where $\mathcal{L}_{\text{Yukawa}}^{\text{SM}}$ is the SM Yukawa interaction, and

$$\mathcal{L}_N = \sum_{\alpha=1}^3 \left(- \sum_{i=1}^3 g_{i\alpha} \bar{L}_i \tilde{\eta} N_\alpha - \frac{y_\alpha^R}{2} \bar{N}_\alpha^c S N_\alpha + \text{h.c.} \right) \quad (2)$$

with $\tilde{\eta} = i\tau^2 \eta^*$, where $i, \alpha = 1, 2, 3$ are flavors of leptons. Without loss of generality, the Yukawa coupling y^R of RH neutrinos can be flavor diagonal. The Yukawa coupling among $\bar{L}_i \Phi N_\alpha$ is prohibited due to the unbroken \mathbb{Z}_2 symmetry. The active neutrinos remain massless at tree level, and obtain tiny masses at one-loop level.

The scalar potential $V(\Phi, \eta, S)$ in this model is given by

$$\begin{aligned} V(\Phi, \eta, S) = & \mu_1^2 |\Phi|^2 + \mu_2^2 |\eta|^2 + \mu_S^2 |S|^2 + \frac{\lambda_1}{2} |\Phi|^4 + \frac{\lambda_2}{2} |\eta|^4 + \lambda_S |S|^4 \\ & + \lambda_3 |\Phi|^2 |\eta|^2 + \lambda_4 \left| \Phi^\dagger \eta \right|^2 + \frac{\lambda_5}{2} \left[(\Phi^\dagger \eta)^2 + \text{h.c.} \right] + \tilde{\lambda} |\Phi|^2 |S|^2 + \lambda |\eta|^2 |S|^2, \end{aligned} \quad (3)$$

where λ_5 can be taken as real by rephasing of the fields. We assume $\mu_1^2 < 0$, $\mu_S^2 < 0$, $\mu_2^2 > 0$, so that Φ and S receive non-zero Vacuum Expectation Values (VEVs) by Spontaneous Symmetry Breaking (SSB) of the $\text{SU}(2)_L \times \text{U}(1)_Y$ and $\text{U}(1)_{B-L}$ gauge symmetries. The VEV of η remains zero.

The $\text{U}(1)_{B-L}$ gauge symmetry is assumed to be spontaneously broken above the electroweak scale. The scalar singlet S is parameterized as

$$S = \frac{1}{\sqrt{2}} (v_S + \phi_S + i z_S), \quad (4)$$

where v_S is the VEV of the $\text{U}(1)_{B-L}$ symmetry breaking, ϕ_S is a neutral scalar boson, and z_S is the Nambu–Goldstone (NG) boson. The Z' boson obtains its mass as $m_{Z'} = 2g_{B-L}v_S$ by its longitudinal mode absorbing z_S , where g_{B-L} is the gauge coupling for the $\text{U}(1)_{B-L}$ symmetry. In the $\text{SU}(2)_L \times \text{U}(1)_Y \times \text{U}(1)_{B-L}$ gauge sector, we suppose that the kinetic mixing between Z and Z' is negligible. RH neutrinos N_α also receive their masses as

$$m_{N_\alpha} = \frac{y_\alpha^R v_S}{\sqrt{2}}. \quad (5)$$

After the Electro-Weak Symmetry Breaking (EWSB), the $\text{SU}(2)_L$ scalar doublet Φ is parameterized as

$$\Phi = \begin{pmatrix} G^+ \\ \frac{1}{\sqrt{2}}(v + \phi + iz) \end{pmatrix}, \quad (6)$$

where v ($\simeq 246$ GeV) is the VEV of the electroweak symmetry breaking, G^+ and z are NG bosons absorbed by longitudinal modes of the electroweak gauge bosons, i.e., W and Z bosons, respectively.

The stationary conditions give the following relations

$$\mu_1^2 + \frac{\lambda_1}{2}v^2 + \frac{\tilde{\lambda}v_S^2}{2} = 0, \quad \mu_S^2 + \lambda_S v_S^2 + \frac{\tilde{\lambda}v^2}{2} = 0. \quad (7)$$

The mixing between ϕ and ϕ_S leads to the following mass terms

$$\frac{1}{2} \begin{pmatrix} \phi & \phi_S \end{pmatrix} \mathcal{M}^2 \begin{pmatrix} \phi \\ \phi_S \end{pmatrix} = \frac{1}{2} \begin{pmatrix} \phi & \phi_S \end{pmatrix} \begin{pmatrix} \lambda_1 v^2 & \tilde{\lambda} v v_S \\ \tilde{\lambda} v v_S & 2\lambda_S v_S^2 \end{pmatrix} \begin{pmatrix} \phi \\ \phi_S \end{pmatrix}. \quad (8)$$

The squared mass matrix \mathcal{M}^2 can be diagonalized by an orthogonal matrix with the mixing angle α

$$\begin{pmatrix} h_1 \\ h_2 \end{pmatrix} = \begin{pmatrix} \cos \alpha & -\sin \alpha \\ \sin \alpha & \cos \alpha \end{pmatrix} \begin{pmatrix} \phi \\ \phi_S \end{pmatrix}, \quad (9)$$

where h_1 and h_2 are mass eigenstates of Higgs bosons

$$m_{h_1}^2 = \lambda_1 v^2 \cos^2 \alpha + 2\lambda_S v_S^2 \sin^2 \alpha - \tilde{\lambda} v v_S \sin 2\alpha, \quad (10)$$

$$m_{h_2}^2 = \lambda_1 v^2 \sin^2 \alpha + 2\lambda_S v_S^2 \cos^2 \alpha + \tilde{\lambda} v v_S \sin 2\alpha, \quad (11)$$

with the constraint

$$\tilde{\lambda} v v_S \cos 2\alpha + \left(\frac{\lambda_1}{2} v^2 - \lambda_S v_S^2 \right) \sin 2\alpha = 0. \quad (12)$$

In this paper, we fix the mass eigenstate h_1 to be the SM-like Higgs boson with $m_{h_1} = 125$ GeV, and h_2 is the additional Higgs boson.

The \mathbb{Z}_2 -odd scalar $\text{SU}(2)_L$ doublet field η can be parameterized as

$$\eta = \begin{pmatrix} H^+ \\ \frac{1}{\sqrt{2}}(H + iA) \end{pmatrix}. \quad (13)$$

The mass spectrum of \mathbb{Z}_2 -odd scalar particles is

$$m_{H^\pm}^2 = \mu_2^2 + \frac{\lambda}{2}v_S^2 + \frac{\lambda_3}{2}v^2, \quad (14)$$

$$m_H^2 = \mu_2^2 + \frac{\lambda}{2}v_S^2 + \frac{\lambda_3 + \lambda_4 + \lambda_5}{2}v^2, \quad (15)$$

$$m_A^2 = \mu_2^2 + \frac{\lambda}{2}v_S^2 + \frac{\lambda_3 + \lambda_4 - \lambda_5}{2}v^2. \quad (16)$$

There are 11 parameters $\mu_1^2, \mu_2^2, \mu_S^2, \lambda_1, \lambda_2, \lambda_3, \lambda_4, \lambda_5, \lambda, \lambda_S, \tilde{\lambda}$ in the scalar potential Eq.(3). They can be replaced by 9 new physics parameters $\mu_2^2, m_{h_2}, m_H, m_A, m_{H^\pm}, \alpha, v_S, \lambda_2$ and λ , in addition to the two SM parameters v and m_{h_1} .

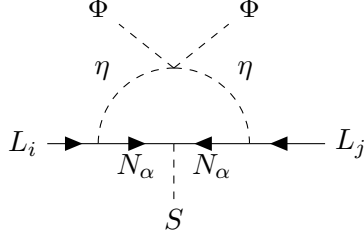


FIG. 1. The one-loop diagram which generates small neutrino masses.

A. Neutrino masses

In this model, tiny neutrino masses are generated via the one-loop induced dimension-six operator $S(\overline{L\Phi})^c L\Phi/\Lambda^2$, where Λ is an energy scale parameter, as shown in FIG. 1.

Following the framework of Ref. [19, 20], after the EWSB, the mass matrix of light neutrinos at one-loop level is

$$m_\nu^{ij} = \sum_\alpha g_{i\alpha} g_{j\alpha} \Lambda_\alpha \equiv (g\Lambda g^T)^{ij}, \quad (17)$$

where the diagonal matrix Λ is defined by

$$\Lambda_\alpha = \frac{m_{N_\alpha}}{32\pi^2} \left[\frac{m_H^2}{m_{N_\alpha}^2 - m_H^2} \ln \left(\frac{m_{N_\alpha}^2}{m_H^2} \right) - \frac{m_A^2}{m_{N_\alpha}^2 - m_A^2} \ln \left(\frac{m_{N_\alpha}^2}{m_A^2} \right) \right]. \quad (18)$$

In order to evaluate the Yukawa coupling of neutrinos, we adopt the Casas-Ibarra (CI) parametrization [41]. The matrix of the Yukawa coupling can be parameterized as

$$g_{i\alpha} = \left(U_{\text{PMNS}} \sqrt{\mathcal{M}_\nu} R \sqrt{\Lambda^{-1}} \right)_{i\alpha}, \quad (19)$$

where U_{PMNS} is the Pontecorvo-Maki-Nakagawa-Sakata matrix [42, 43], and the diagonalized mass matrix of active neutrinos is defined as $\mathcal{M}_\nu \equiv \text{diag}(m_{\nu_1}, m_{\nu_2}, m_{\nu_3})$. The matrix R is an arbitrary complex orthogonal matrix. We take $R = I$ in the following analysis.

III. CONSTRAINTS ON THE MODEL

In this section, we discuss possible theoretical and experimental constraints in this model. We consider perturbativity and vacuum stability as theoretical constraints. We consider experimental constraints from neutrino oscillations, collider experiments, flavor experiments, dark matter observations as well as the electroweak precision tests.

A. Theoretical constraints

In this subsection, we consider theoretical bounds in the model: perturbativity and vacuum stability. Perturbativity requires that all the quartic vertices of scalar fields should satisfy the perturbativity criterion $\lambda_1, \lambda_2, \lambda_3, \lambda_4, \lambda_5, \lambda_S, \tilde{\lambda}, \lambda < 4\pi$, and Yukawa couplings should satisfy $(y_1^R)^2, (y_2^R)^2, (y_3^R)^2 < 4\pi$.

Next, vacuum stability at tree level requires that the scalar potential is bounded from below in all the directions of the field space [44–53]. Therefore, the vacuum stability requires

$$\begin{aligned} \lambda_1 &\geq 0, \quad \lambda_2 \geq 0, \quad \lambda_3 \geq -\sqrt{\lambda_1 \lambda_2}, \quad \lambda_3 + \lambda_4 \pm \lambda_5 \geq -\sqrt{\lambda_1 \lambda_2}, \\ \lambda_S &\geq 0, \quad \lambda \geq -\sqrt{2}\sqrt{\lambda_2 \lambda_S}, \quad \tilde{\lambda} \geq -\sqrt{2}\sqrt{\lambda_1 \lambda_S}. \end{aligned} \quad (20)$$

B. Constraints from experiments

First, we discuss constraints from neutrino oscillation. We consider normal mass ordering of neutrinos, and adopt the latest data from the PDG [39], so our analysis is compatible with neutrino oscillation measurements:

$$\begin{aligned} \Delta m_{21}^2 &= (7.53 \pm 0.18) \times 10^{-5} \text{ eV}^2, \quad \Delta m_{23}^2 = (2.455 \pm 0.028) \times 10^{-3} \text{ eV}^2, \quad \delta_{CP} = (1.19 \pm 0.22)\pi, \\ \sin^2(\theta_{12}) &= 0.307 \pm 0.013, \quad \sin^2(\theta_{13}) = 0.0219 \pm 0.0007, \quad \sin^2(\theta_{23}) = 0.558 \pm 0.015. \end{aligned} \quad (21)$$

Next, we consider constraints from lepton flavor violation (LFV). In this model, LFV decay processes can be achieved via one-loop diagrams mediated by H^\pm and N_α . We consider constraints from $\ell_i \rightarrow \ell_j \gamma$ and $\ell_i \rightarrow \ell_j \ell_k \bar{\ell}_k$, as shown in Table II.

Third, this model basically provides two candidates of DM, which are the lightest RH neutrino or the lightest neutral \mathbb{Z}_2 odd scalar particle. The relic density of DM candidates should satisfy observation results from the Planck satellite $\Omega h^2 = 0.120 \pm 0.001$ [2]. Direct detection (DD) experiments can also give constraints to this model. We apply limits from the LZ experiment [40] on the WIMP-nucleon spin independent elastic scattering cross section. Detailed analysis is shown in the next section.

Fourth, collider experiments give rich constraints on this model, including masses of new particles (e.g. Z' , m_{h_2} , inert scalar particles) and BSM parameters (e.g. α and v_S). The LEP II experiment gives the lower limit of the ratio between the mass of Z' gauge boson and its coupling constant $m_{Z'}/g_{B-L} > 7 \text{ TeV}$ [31, 56, 57]. Chargino searches at the LEP II experiment can provide a limit of $m_{H^\pm} > 80 \text{ GeV}$ [32]. The LEP II experiment also exclude the intersection of the following

| LFV processes | Current bounds on branching ratios |
|---|------------------------------------|
| $\mu^+ \rightarrow e^+ \gamma$ | 3.1×10^{-13} [26] |
| $\mu^+ \rightarrow e^- e^+ e^-$ | 1.0×10^{-12} [27] |
| $\tau^+ \rightarrow e^+ \gamma$ | 3.3×10^{-8} [28] |
| $\tau^+ \rightarrow \mu^+ \gamma$ | 4.2×10^{-8} [29] |
| $\tau^- \rightarrow e^- e^+ e^-$ | 2.7×10^{-8} [30] |
| $\tau^- \rightarrow e^+ \mu^- \mu^-$ | 1.7×10^{-8} [30] |
| $\tau^- \rightarrow e^- \mu^+ \mu^-$ | 2.7×10^{-8} [30] |
| $\tau^- \rightarrow \mu^+ e^- e^-$ | 1.5×10^{-8} [30] |
| $\tau^- \rightarrow \mu^- e^+ e^-$ | 1.8×10^{-8} [30] |
| $\tau^- \rightarrow \mu^- \mu^+ \mu^-$ | 2.1×10^{-8} [30] |
| $\mu^- \text{Ti} \rightarrow e^- \text{Ti}$ | 4.3×10^{-12} [54] |
| $\mu^- \text{Au} \rightarrow e^- \text{Au}$ | 7.0×10^{-13} [55] |

TABLE II. Current experimental bounds for LFV processes.

mass region for inert scalar particles [58]:

$$m_H < 80 \text{ GeV}, \quad m_A < 100 \text{ GeV}, \quad m_A - m_H > 8 \text{ GeV}. \quad (22)$$

With precise measurements of decay widths of W and Z bosons [39], kinematically allowed regions for decay processes $W/Z \rightarrow \eta\eta$ are excluded. The null result in searching for the Z' boson at ATLAS [33, 34] and CMS [35, 36] gives strong constraints on the Z' boson, $m_{Z'} < 5.15 \text{ TeV}$. Precise measurements for the Higgs boson couplings give constraints on the mixing between ϕ and ϕ_S . The scaling factor for the $h_1 ZZ$ coupling is given by

$$\kappa_Z^2 \equiv \frac{\Gamma(h_1 \rightarrow ZZ)}{\Gamma_{\text{SM}}(h_1 \rightarrow ZZ)} = \cos^2 \alpha, \quad (23)$$

where ATLAS [37] and CMS [38] provide

$$\kappa_Z = 1.04 \pm 0.07, \quad (24)$$

from which we obtain $0.90 < \cos \alpha \leq 1.0$ as a criterion of 95% CL ¹.

Finally, we will consider constraints from the electroweak precision test. Electroweak precision measurements can provide strong constraints on BSM physics. The oblique parameter T gives the strongest constraint on a multi-Higgs scenario among S, T, U parameters [61, 62]. In this model,

¹ The allowed parameter space for m_{h_2} and α is shown in Ref. [59, 60] from the direct search results for h_2 .

inert doublet field and scalar singlet field contribute to deviations of T [63–65]:

$$\Delta T = \frac{3 \sin^2 \alpha}{16 \pi s_W^2} \left[f_T \left(\frac{m_{h_2}^2}{m_W^2} \right) - f_T \left(\frac{m_{h_1}^2}{m_W^2} \right) - \frac{1}{c_W^2} \left(f_T \left(\frac{m_{h_2}^2}{m_Z^2} \right) - f_T \left(\frac{m_{h_1}^2}{m_Z^2} \right) \right) \right] + \frac{1}{16 \pi m_W^2 s_W^2} [F(m_{H^\pm}, m_H) + F(m_{H^\pm}, m_A) - F(m_H, m_A)], \quad (25)$$

where $c_W^2 \equiv m_W^2/m_Z^2$ and $s_W^2 = 1 - c_W^2$. The auxiliary functions are defined as

$$F(x, y) = \frac{x^2 + y^2}{2} - \frac{x^2 y^2}{x^2 - y^2} \ln \frac{x^2}{y^2}, \quad f_T(x) = \frac{x \log x}{x - 1}. \quad (26)$$

IV. LEPTON FLAVOR VIOLATION

In this section, we consider constraints from LFV. LFV processes can be enhanced through N_α – H^\pm loop diagrams in this model. The branching ratio for $\ell_i \rightarrow \ell_j \gamma$ is calculated as

$$\text{Br}(\ell_i \rightarrow \ell_j \gamma) = \frac{48 \pi^3 \alpha_{\text{em}} |A_D|^2}{G_F^2} \text{Br}(\ell_i \rightarrow \ell_j \bar{\nu}_j \nu_i), \quad (27)$$

with

$$A_D = \sum_\alpha \frac{i g_{i\alpha}^* g_{j\alpha}}{32 \pi^2 m_{H^\pm}^2} F(\xi_\alpha), \quad (28)$$

where ξ_α is defined as $\xi_\alpha \equiv m_{N_\alpha}^2/m_{H^\pm}^2$, α_{em} is the fine structure constant, G_F is the Fermi constant, and the function $F(x)$ is defined as

$$F(x) = \frac{1 - 6x + 3x^2 + 2x^3 - 6x^2 \ln x}{6(x - 1)^4}. \quad (29)$$

$\ell_i \rightarrow \ell_j \ell_k \bar{\ell}_k$ processes include photon penguin diagrams and box diagrams. The branching ratios of photon penguin diagrams can have a simple relation with the radiative decay processes [66–68]:

$$\text{Br}(\ell_i \rightarrow \ell_j \ell_j \bar{\ell}_j) \simeq \frac{\alpha_{\text{em}}}{3\pi} \left[2 \log \left(\frac{m_{\ell_i}}{m_{\ell_j}} \right) - \frac{11}{4} \right] \text{Br}(\ell_i \rightarrow \ell_j \gamma), \quad (30)$$

$$\text{Br}(\ell_i \rightarrow \ell_j \ell_k \bar{\ell}_k) \simeq \frac{\alpha_{\text{em}}}{3\pi} \left[2 \log \left(\frac{m_{\ell_i}}{m_{\ell_j}} \right) - 3 \right] \text{Br}(\ell_i \rightarrow \ell_j \gamma) \quad (j \neq k). \quad (31)$$

The box diagrams can be dominant when $\xi \gg 1$ or $\xi \ll 1$ if masses of RH neutrinos are degenerate. $\mu \rightarrow e$ conversion in muonic atoms is also a signature of LFV. However, $\mu \rightarrow e \gamma$ is more stringent than this process [68]. Detailed analysis of LFV can be seen in Ref. [66–69].

Considering the constraints from neutrino oscillations and LFV measurements, we choose the following parameters for later use:

$$m_{N_2} = m_{N_1} + 2500 \text{ GeV}, \quad m_{N_3} = m_{N_1} + 3000 \text{ GeV}, \quad m_H = 1000 \text{ GeV}, \\ m_{H^\pm} = m_A, \quad \delta \equiv m_{H^\pm} - m_H = 10^{-5} \text{ GeV}. \quad (32)$$

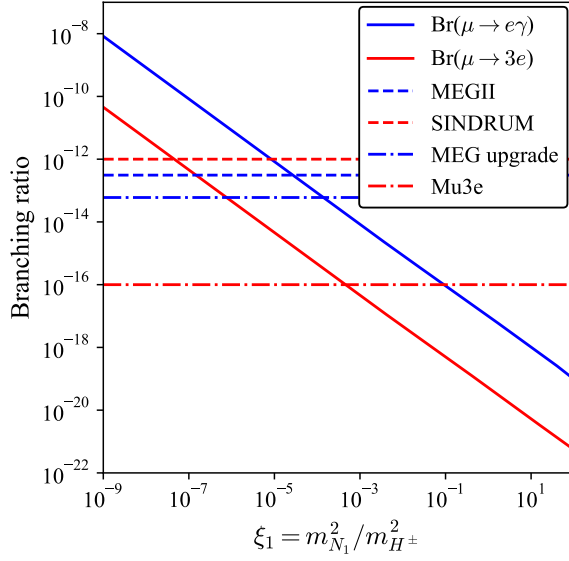


FIG. 2. $\text{Br}(\mu \rightarrow e\gamma)$ (blue) and $\text{Br}(\mu \rightarrow 3e)$ (red) as a function of $\xi = m_{N_1}^2/m_{H^\pm}^2$. Horizontal dashed lines show the current upper bounds from MEGII experiment (blue) [26] and SINDRUM experiment (red) [27]. The dot-dashed lines show the future bounds from MEG upgrade (blue) [70] and Mu3e (red) [71].

LFV constraints on the mass of N_1 is shown in FIG. 2. The blue (red) solid line shows $\text{Br}(\mu \rightarrow e\gamma)$ ($\text{Br}(\mu \rightarrow 3e)$). The horizontal dashed blue and red lines are current upper bounds from MEGII [70] and SINDRUM [71], respectively. Future expected bounds from MEG upgrade [70] and Mu3e [71] are shown as dot-dashed lines. As m_{N_1} is increasing, branching ratios of LFV processes are decreasing, which provides the lower bound of m_{N_1} around $m_{N_1} \simeq 5.1$ GeV.

V. DARK MATTER

In this section, we consider the freeze-out mechanism for DM candidates. The relic abundance of the DM particle can be calculated by solving the Boltzmann equation [72]:

$$\frac{dY}{dx} = -\sqrt{\frac{g_*\pi}{45}} \frac{m_{\text{DM}} m_{\text{Pl}}}{x^2} \langle \sigma v \rangle (Y^2 - Y_{\text{EQ}}^2), \quad (33)$$

where $x \equiv m_{\text{DM}}/T$ is an independent variable, $Y \equiv n_{\text{DM}}/s$ is the comoving density of DM. The thermal averaged cross section $\langle \sigma v \rangle$ contains cross sections of all annihilation processes before the DM freezes out. Integrating the Boltzmann equation from $x = 0$ to $x_F = m_{\text{DM}}/T_F$, the relic abundance is given by

$$\Omega_{\text{DM}} h^2 \simeq 2.75 \times 10^{-8} m_{\text{DM}} Y(T_F) \text{GeV}^{-1}, \quad (34)$$

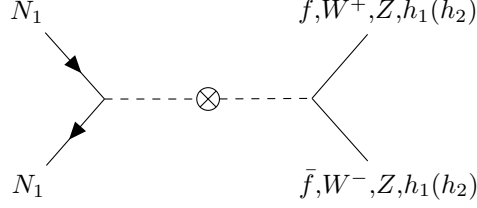


FIG. 3. Annihilation processes $N_1 N_1 \rightarrow h_1(h_2) \rightarrow f \bar{f}, ZZ, W^+ W^-, h_1(h_2) h_1(h_2)$ through the mixing between ϕ and ϕ_S .

where T_F is the freeze-out temperature of DM.

In this paper, we discuss two scenarios for two DM candidates. We first discuss fermionic DM scenario where N_1 is the lightest particle in the \mathbb{Z}_2 odd sector, and show allowed parameter spaces under current various experiments. We then briefly discuss scalar DM scenario in the model, whose discussions are similar to several previous studies [58, 73–76]. In the following analysis, we use the numerical analysis package micrOMEGAs 6.0 [77] to calculate the relic abundance of DM.

A. N_1 dark matter

In this scenario, we consider N_1 as the lightest \mathbb{Z}_2 odd particle.

First, we consider the relic abundance of N_1 dark matter. In the Tao-Ma model [19, 20], there is no sufficient annihilation rates for N_1 DM due to strong constraints from LFV experiments [78]. However, it is possible for N_1 to satisfy the DM abundance with the mixing between the Higgs field Φ and the extra scalar singlet S , because N_1 can annihilate via $N_1 N_1 \rightarrow h_1(h_2) \rightarrow f \bar{f}, ZZ, W^+ W^-, h_1(h_2) h_1(h_2)$ processes [23], as shown in FIG. 3.

In FIG.4, the relic abundance of N_1 is shown as a function of m_{N_1} . We use the following parameters to calculate the relic abundance:

$$\begin{aligned}
 \cos \alpha &= 0.97, \quad v_S = 30 \text{ TeV}, \quad m_{h_2} = 200 \text{ GeV}, \quad m_{Z'} = 5.2 \text{ TeV}, \\
 m_{N_2} &= m_{N_1} + 2500 \text{ GeV}, \quad m_{N_3} = m_{N_1} + 3000 \text{ GeV}, \quad \lambda = 10^{-6}, \quad \lambda_3 = 0.1, \\
 m_H &= m_{N_1} + 10^3 \text{ GeV}, \quad m_{H^\pm} = m_A = m_H + 10^{-5} \text{ GeV}.
 \end{aligned} \tag{35}$$

The relic abundance of N_1 is reduced significantly around $m_{N_1} \simeq m_{h_1}/2$ and $m_{N_1} \simeq m_{h_2}/2$, respectively. Annihilations of RH neutrinos to the SM particles are enhanced resonantly via s -channel exchange of h_1 and h_2 . We also notice that it is possible for RH neutrinos to annihilate via Z' boson exchange. However, this process is not dominant since the cross section of Z' boson

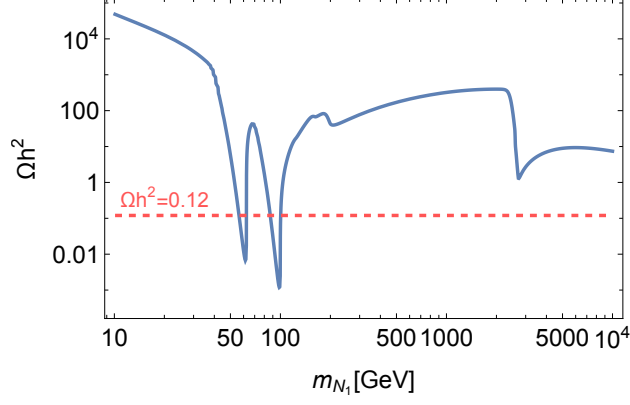


FIG. 4. Relic abundance of N_1 as a function of m_{N_1} . The red dashed line is the current bound of DM relic abundance from the Planck experiment [2].

exchange $\langle\sigma v\rangle$ is proportional to $1/v_S^4$, which is much smaller than Higgs boson exchange processes in the low mass region $m_{N_1} \ll m_{Z'}/2$. In the mass region near the Z' pole $m_{N_1} \simeq m_{Z'}/2$, even if annihilations can be enhanced due to Z' resonance, it cannot realize the required relic abundance.

Second, we consider the direct detection (DD) of N_1 dark matter. The lightest RH neutrino N_1 can have elastic scattering with nucleons by Higgs exchange processes. The spin independent (SI) cross section for the proton target is

$$\sigma_{\text{SI}}^p = \frac{4\mu^2}{\pi} f_p^2, \quad (36)$$

where $\mu \equiv \frac{m_{N_1} m_p}{m_{N_1} + m_p}$ is the DM-nucleus reduced mass in the center of mass frame. The hadronic matrix element f_p [79] is given by

$$f_p = \sum_{q=u,d,s} c_q \frac{m_p}{m_q} f_{Tq}^p + \frac{2}{27} f_{TG}^p \sum_{q=c,b,t} c_q \frac{m_p}{m_q}, \quad (37)$$

where f_{Tq}^p and f_{TG}^p express mass contributions to the nucleon from quarks and gluons, and m_q is the mass of a quark with a Yukawa coupling y_q . The effective vertex c_q is defined as

$$c_q = y_R^\alpha y_q \left[\left(\frac{\sin \alpha}{\sqrt{2}} \right) \frac{1}{m_{h_1}^2} \left(\frac{\cos \alpha}{\sqrt{2}} \right) - \left(\frac{\sin \alpha}{\sqrt{2}} \right) \frac{1}{m_{h_2}^2} \left(\frac{\cos \alpha}{\sqrt{2}} \right) \right]. \quad (38)$$

The spin independent cross section σ_{SI}^p has a simple relation with BSM parameters in this model:

$$\sigma_{\text{SI}}^p \propto \left(\frac{m_{N_1} \sin(2\alpha)}{v_S} \right)^2 \times \left(\frac{1}{m_{h_1}^2} - \frac{1}{m_{h_2}^2} \right)^2. \quad (39)$$

In FIG. 5, the relic abundance of N_1 DM is shown as colored contour in the v_S - α plane. We

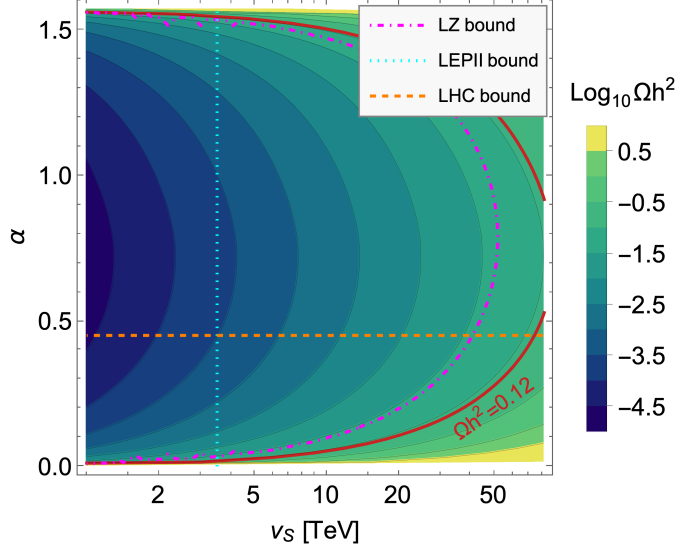


FIG. 5. Parameter space of $m_{N_1} = 100.1$ GeV with constraints from LEP II [31, 56], ATLAS [37], CMS [38] and LZ [40] experiments. The red line is the bound from the Planck experiment [2].

choose the following parameter set:

$$\begin{aligned}
 m_{N_1} &= 100.1 \text{ GeV}, \quad m_{h_2} = 200 \text{ GeV}, \quad m_{N_2} = 2500 \text{ GeV}, \quad m_{N_3} = 3000 \text{ GeV}, \\
 \lambda &= 10^{-6}, \quad \lambda_3 = 0.1, \quad m_H = 1000 \text{ GeV}, \quad m_{H^\pm} = m_A, \quad \delta \equiv m_{H^\pm} - m_H = 10^{-5} \text{ GeV}.
 \end{aligned} \tag{40}$$

The allowed parameter space is the region encircled by the LZ 2022 [40] (magenta dot-dashed), LHC [37, 38] (orange dashed) and Planck experiment [2] (red solid), which is on the right side of the LEP II constraint [31, 56] (cyan dotted). We also investigate the parameter space of the SM-like Higgs resonance near the region $m_{N_1} \simeq m_{h_1}/2$. We find that there are still parameter spaces for N_1 DM with the SM-like Higgs resonance if m_{h_2} is near m_{h_1} .

Third, we explore the allowed mass region of N_1 with h_2 resonance scenario. We choose the following parameter space

$$\cos \alpha \in [0.9, 1], \quad v_S \in [3.5, 80] \text{ TeV}, \quad m_{h_2} \in [10, 10^4] \text{ GeV} \tag{41}$$

with

$$\begin{aligned}
 m_{N_2} &= m_{N_1} + 2500 \text{ GeV}, \quad m_{N_3} = m_{N_1} + 3000 \text{ GeV}, \quad m_{h_2} = 2m_{N_1} + 0.4 \text{ GeV}, \\
 \lambda &= 10^{-6}, \quad \lambda_3 = 0.1, \quad m_H = m_{N_1} + 10^3 \text{ GeV}, \quad m_{H^\pm} = m_A = m_H + 10^{-5} \text{ GeV}.
 \end{aligned} \tag{42}$$

We scan $\cos \alpha$, v_S and m_{h_2} with $20 \times 20 \times 100$ points, respectively. The allowed parameter space of N_1 is shown in FIG. 6, in which all points satisfy the constraint $\Omega_{\text{DM}} h^2 < 0.12$. Blue points

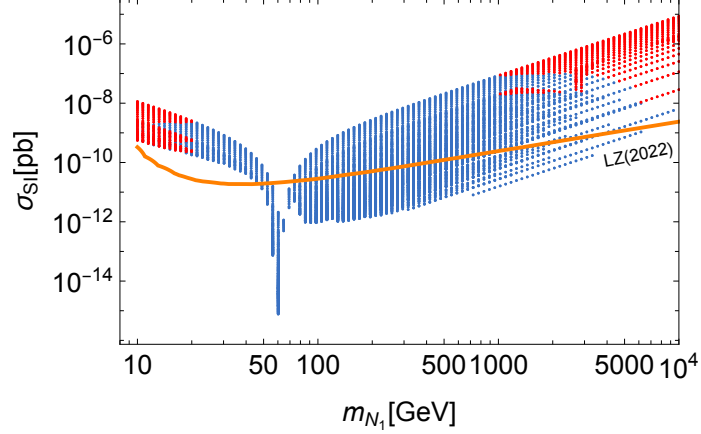


FIG. 6. Possible SI cross section of N_1 as a function of m_{N_1} in our parameter space. Red points are excluded by theoretical constraints. The orange line is the upper bound from the LZ experiment [40].

satisfy all theoretical and experimental constraints, while red points are excluded by theoretical constraints. The low mass region $m_{N_1} \lesssim 45$ GeV is excluded by the LZ experiment since the SI cross section rapidly increases due to the large contribution of h_2 exchange processes. In the mass region near $m_{N_1} \simeq m_{h_1}/2$, the SI cross section greatly reduces due to the destructive interference of the two Higgs states. In high mass regions $m_{N_1} \gtrsim 80$ GeV, the SI cross section increases as m_{N_1} is increasing. However, there is still allowed mass region for N_1 DM. In the region $m_{N_1} > 5$ TeV, the SI cross section exceeds the LZ bound again, therefore current direct detection experiments can give the lower and upper bounds on the mass of N_1 .

B. Scalar dark matter

In this scenario, we consider H is the lightest \mathbb{Z}_2 odd particle. The H DM scenario has been studied extensively in the inert doublet model [58, 73, 74, 80, 81]. In our model, there are two differences with the inert doublet model. Discussions of H DM is similar to the inert doublet model with an additional scalar singlet [75, 76].

First, the relic density can be satisfied by the additional Higgs resonance near the mass region $m_H \simeq m_{h_2}/2$. H can annihilate via $HH \rightarrow h_1(h_2) \rightarrow f\bar{f}, W^+W^-, ZZ, h_1(h_2)h_1(h_2)$ processes.

Second, the SI cross section in direct detections can be changed due to the h_2 exchange processes. The SI cross section of H is given by

$$\sigma_{\text{SI}}^H = \frac{\mu_H^2}{4\pi m_H^2} f_p^2, \quad \mu_H \equiv \frac{m_H m_p}{m_H + m_p}, \quad (43)$$

where f_p has the same definition as Eq. (37), and c_q is defined as ²

$$c_q = \frac{y_q}{2\sqrt{2}} \left[\frac{\lambda v_S \sin \alpha \cos \alpha - \lambda_L v \cos^2 \alpha}{m_{h_1}^2} - \frac{\lambda_L v \sin^2 \alpha + \lambda v_S \sin \alpha \cos \alpha}{m_{h_2}^2} \right]. \quad (44)$$

We here take a benchmark point for the H DM scenario:

$$\begin{aligned} v_S = 5 \text{ TeV}, \mu_2^2 = 3460 \text{ GeV}^2, m_{h_2} = 120 \text{ GeV}, \cos \alpha = 0.98, \lambda = 10^{-4}, m_{H^\pm} = 100 \text{ GeV}, \\ m_H = 60 \text{ GeV}, m_A = 100 \text{ GeV}, m_{N_1} = 3000 \text{ GeV}, m_{N_2} = 3500 \text{ GeV}, m_{N_3} = 4000 \text{ GeV}. \end{aligned} \quad (45)$$

The SI cross section and the LZ value of this point are given by

$$\sigma_{\text{SI}}^H = 5.35 \times 10^{-12} \text{ pb}, \sigma_{\text{LZ}(2022)} = 2.01 \times 10^{-11} \text{ pb}. \quad (46)$$

The relic abundance of this benchmark point is evaluated to be

$$\Omega_{\text{DM}} h^2 \simeq 0.12, \quad (47)$$

indicating that there is still allowed parameter space for the H DM scenario in this model.

VI. DISCUSSIONS

In this section, we give some comments on the results shown in section IV and V. In section IV, we have shown that experiment results give the lower bound of m_{N_1} . At present, the most stringent constraint comes from the $\mu \rightarrow e\gamma$ process, which gives the lower bound on $m_{N_1} > 5.2 \text{ GeV}$ in our N_1 DM scenario. In the future, the MEG experiment [70] may improve its sensitivity down to $\text{Br}(\mu \rightarrow e\gamma) \simeq 6 \times 10^{-14}$, and the Mu3e experiment [71] may upgrade the sensitivity to $\text{Br}(\mu \rightarrow 3e) \simeq 1 \times 10^{-16}$. Future LFV experiments would give the lower bound $m_{N_1} > 21 \text{ GeV}$ in our N_1 DM scenario, which is 4 times better than the current bound.

In section V, we have shown benchmark points and parameter space of DM candidates in this model. Knowing the allowed parameter spaces, we can discuss the testability of new particles at future collider experiments. We here very briefly mention the prospect for collider searches in each scenario. In the N_1 DM scenario, N_1 could be tested through $H^\pm \rightarrow l^\pm N_1$ signals at LHC and HL-LHC if it is kinematically allowed, mainly via $pp \rightarrow H^+ H^- \rightarrow N_1 N_1 l^+ l^-$ [73, 80, 83–86]. In the H DM scenario, inert scalar particles can be produced through monojet processes (e.g., $q\bar{q} \rightarrow Zg \rightarrow H A j$ and $q\bar{q} \rightarrow h_1 g \rightarrow H H g$) in hadron colliders. A and H^\pm can decay to

² The SI cross section can be modified depending on the size of λ_2 via loop corrections [82].

H via weak interactions. Cross sections of processes including the ZHA vertex only depend on m_H and m_A . Cross section of processes including the h_1HH vertex not only depend on m_H , but also the dimensionless parameter $\lambda_3 + \lambda_4 + \lambda_5$. Detailed analysis of inert scalars in the LHC can be found in Ref. [73, 84, 86]. Inert scalars can also be produced in lepton colliders through $e^+e^- \rightarrow Z \rightarrow AH(H^+H^-)$ processes [80, 85].

The existence of the Z' boson is another difference from the Tao-Ma model. Though searches in the LHC give strong constraints on the mass of Z' boson, it can be lighter with smaller gauge couplings. Since hadron colliders (e.g., LHC and HL-LHC) have large backgrounds, it can only reach the gauge coupling g_{B-L} of $\mathcal{O}(10^{-2})$ [87]. However, lepton colliders (e.g., ILC) can reach smaller gauge coupling of $\mathcal{O}(10^{-3})$ [87]. Decays of the Z' boson into SM particles are proportional to $(B-L)^2$. Due to its large mass, the branching ratios of $Z' \rightarrow q\bar{q}, l^+l^-, \nu_L\bar{\nu}_L, N_1N_1, h_1h_1, h_1h_2$ and h_2h_2 for the parameter set Eq. (35) are given approximately by 0.20, 0.29, 0.15, 0.15, 6.9×10^{-4} , 4.4×10^{-2} , 0.17, respectively [22, 56].

Direct detection experiments become more and more stringent for DM candidates. The LZ collaboration has released its preliminary result with 280 days of data in 2024 [88], which has improved a lot compared to the LZ 2022 result [40]. Future DM detection experiments may give stronger bounds on the DM mass in this model.

VII. CONCLUSIONS

The radiative seesaw model with gauged $U(1)_{B-L} \times \mathbb{Z}_2$ extension is a well-motivated scenario which gives consistent predictions of active neutrino masses and the abundance of dark matter. Majorana masses of right-handed neutrinos, the lightest of which can be identified as dark matter, are given by the spontaneous breaking of the $U(1)_{B-L}$ gauge symmetry. We have revisited this model with the latest constraints from dark matter searches, neutrino oscillations, flavor experiments and collider experiments. We have explored the feasible parameter space of this model, and have found that there is still allowed region for this model under the latest experimental constraints. We have presented new viable benchmark scenarios for this model, i.e., the right-handed neutrino dark matter scenario and the scalar dark matter scenario. We also have mentioned the testability of these benchmark scenarios at future experiments.

ACKNOWLEDGEMENTS

The work of S. K. was supported by the JSPS Grants-in-Aid for Scientific Research No. 20H00160, No. 23K17691 and No. 24KF0060. The work of Y. M. was supported by the JSPS Grant-in-Aid for JSPS Fellows No. 23KJ1460. The work of G. Y. was supported by the PhD support program for Pioneering Quantum Beam Applications (PQBA) and the Nishimura International Scholarship foundation.

-
- [1] Y. Fukuda et al. Evidence for oscillation of atmospheric neutrinos. *Phys. Rev. Lett.*, 81:1562–1567, 1998.
 - [2] N. Aghanim et al. Planck 2018 results. VI. Cosmological parameters. *Astron. Astrophys.*, 641:A6, 2020. [Erratum: *Astron. Astrophys.* 652, C4 (2021)].
 - [3] Benjamin W. Lee and Steven Weinberg. Cosmological Lower Bound on Heavy Neutrino Masses. *Phys. Rev. Lett.*, 39:165–168, 1977.
 - [4] Gerard Jungman, Marc Kamionkowski, and Kim Griest. Supersymmetric dark matter. *Phys. Rept.*, 267:195–373, 1996.
 - [5] Peter Minkowski. $\mu \rightarrow e\gamma$ at a Rate of One Out of 10^9 Muon Decays? *Phys. Lett. B*, 67:421–428, 1977.
 - [6] Tsutomu Yanagida. Horizontal gauge symmetry and masses of neutrinos. *Conf. Proc. C*, 7902131:95–99, 1979.
 - [7] Murray Gell-Mann, Pierre Ramond, and Richard Slansky. Complex Spinors and Unified Theories. *Conf. Proc. C*, 790927:315–321, 1979.
 - [8] Pierre Ramond. The Family Group in Grand Unified Theories. In *International Symposium on Fundamentals of Quantum Theory and Quantum Field Theory*, 2 1979.
 - [9] T. P. Cheng and Ling-Fong Li. Neutrino Masses, Mixings and Oscillations in $SU(2) \times U(1)$ Models of Electroweak Interactions. *Phys. Rev. D*, 22:2860, 1980.
 - [10] J. Schechter and J. W. F. Valle. Neutrino Masses in $SU(2) \times U(1)$ Theories. *Phys. Rev. D*, 22:2227, 1980.
 - [11] George Lazarides, Q. Shafi, and C. Wetterich. Proton Lifetime and Fermion Masses in an $SO(10)$ Model. *Nucl. Phys. B*, 181:287–300, 1981.
 - [12] Rabindra N. Mohapatra and Goran Senjanovic. Neutrino Masses and Mixings in Gauge Models with Spontaneous Parity Violation. *Phys. Rev. D*, 23:165, 1981.
 - [13] M. Magg and C. Wetterich. Neutrino Mass Problem and Gauge Hierarchy. *Phys. Lett. B*, 94:61–64, 1980.
 - [14] Robert Foot, H. Lew, X. G. He, and Girish C. Joshi. Seesaw Neutrino Masses Induced by a Triplet of Leptons. *Z. Phys. C*, 44:441, 1989.

- [15] A. Zee. A Theory of Lepton Number Violation, Neutrino Majorana Mass, and Oscillation. *Phys. Lett. B*, 93:389, 1980. [Erratum: *Phys.Lett.B* 95, 461 (1980)].
- [16] A. Zee. Quantum Numbers of Majorana Neutrino Masses. *Nucl. Phys. B*, 264:99–110, 1986.
- [17] K. S. Babu. Model of ‘Calculable’ Majorana Neutrino Masses. *Phys. Lett. B*, 203:132–136, 1988.
- [18] Lawrence M. Krauss, Salah Nasri, and Mark Trodden. A Model for neutrino masses and dark matter. *Phys. Rev. D*, 67:085002, 2003.
- [19] Zhi-jian Tao. Radiative seesaw mechanism at weak scale. *Phys. Rev. D*, 54:5693–5697, 1996.
- [20] Ernest Ma. Verifiable radiative seesaw mechanism of neutrino mass and dark matter. *Phys. Rev. D*, 73:077301, 2006.
- [21] Mayumi Aoki, Shinya Kanemura, and Osamu Seto. Neutrino mass, Dark Matter and Baryon Asymmetry via TeV-Scale Physics without Fine-Tuning. *Phys. Rev. Lett.*, 102:051805, 2009.
- [22] Shinya Kanemura, Osamu Seto, and Takashi Shimomura. Masses of dark matter and neutrino from TeV scale spontaneous $U(1)_{B-L}$ breaking. *Phys. Rev. D*, 84:016004, 2011.
- [23] Nobuchika Okada and Osamu Seto. Higgs portal dark matter in the minimal gauged $U(1)_{B-L}$ model. *Phys. Rev. D*, 82:023507, 2010.
- [24] Debasish Borah, Dibyendu Nanda, Nimmala Narendra, and Narendra Sahu. Right-handed neutrino dark matter with radiative neutrino mass in gauged $B - L$ model. *Nucl. Phys. B*, 950:114841, 2020.
- [25] Osamu Seto and Takashi Shimomura. Atomki anomaly and dark matter in a radiative seesaw model with gauged $B - L$ symmetry. *Phys. Rev. D*, 95(9):095032, 2017.
- [26] K. Afanaciev et al. A search for $\mu^+ \rightarrow e^+ \gamma$ with the first dataset of the MEG II experiment. *Eur. Phys. J. C*, 84(3):216, 2024.
- [27] U. Bellgardt et al. Search for the Decay $\mu^+ \rightarrow e^+ e^+ e^-$. *Nucl. Phys. B*, 299:1–6, 1988.
- [28] Bernard Aubert et al. Searches for Lepton Flavor Violation in the Decays $\tau^\pm \rightarrow e^\pm \gamma$ and $\tau^\pm \rightarrow \mu^\pm \gamma$. *Phys. Rev. Lett.*, 104:021802, 2010.
- [29] A. Abdesselam et al. Search for lepton-flavor-violating tau-lepton decays to $\ell \gamma$ at Belle. *JHEP*, 10:19, 2021.
- [30] K. Hayasaka et al. Search for Lepton Flavor Violating τ Decays into Three Leptons with 719 Million Produced $\tau^+ \tau^-$ Pairs. *Phys. Lett. B*, 687:139–143, 2010.
- [31] the SLD Electroweak. A Combination of preliminary electroweak measurements and constraints on the standard model. 12 2003.
- [32] G. Abbiendi et al. Search for Charged Higgs bosons: Combined Results Using LEP Data. *Eur. Phys. J. C*, 73:2463, 2013.
- [33] Georges Aad et al. Search for high-mass dilepton resonances using 139 fb $^{-1}$ of pp collision data collected at $\sqrt{s} = 13$ TeV with the ATLAS detector. *Phys. Lett. B*, 796:68–87, 2019.
- [34] Georges Aad et al. Search for new resonances in mass distributions of jet pairs using 139 fb $^{-1}$ of pp collisions at $\sqrt{s} = 13$ TeV with the ATLAS detector. *JHEP*, 03:145, 2020.

- [35] Albert M Sirunyan et al. Search for resonant and nonresonant new phenomena in high-mass dilepton final states at $\sqrt{s} = 13$ TeV. *JHEP*, 07:208, 2021.
- [36] Armen Tumasyan et al. Search for narrow resonances in the b-tagged dijet mass spectrum in proton-proton collisions at $\sqrt{s} = 13$ TeV. *Phys. Rev. D*, 108(1):012009, 2023.
- [37] Georges Aad et al. A detailed map of Higgs boson interactions by the ATLAS experiment ten years after the discovery. *Nature*, 607(7917):52–59, 2022. [Erratum: *Nature* 612, E24 (2022)].
- [38] Armen Tumasyan et al. A portrait of the Higgs boson by the CMS experiment ten years after the discovery. *Nature*, 607(7917):60–68, 2022. [Erratum: *Nature* 623, (2023)].
- [39] R. L. Workman et al. Review of Particle Physics. *PTEP*, 2022:083C01, 2022.
- [40] J. Aalbers et al. First Dark Matter Search Results from the LUX-ZEPLIN (LZ) Experiment. *Phys. Rev. Lett.*, 131(4):041002, 2023.
- [41] J. A. Casas and A. Ibarra. Oscillating neutrinos and $\mu \rightarrow e, \gamma$. *Nucl. Phys. B*, 618:171–204, 2001.
- [42] B. Pontecorvo. Inverse beta processes and nonconservation of lepton charge. *Zh. Eksp. Teor. Fiz.*, 34:247, 1957.
- [43] Ziro Maki, Masami Nakagawa, and Shoichi Sakata. Remarks on the unified model of elementary particles. *Prog. Theor. Phys.*, 28:870–880, 1962.
- [44] Nilendra G. Deshpande and Ernest Ma. Pattern of Symmetry Breaking with Two Higgs Doublets. *Phys. Rev. D*, 18:2574, 1978.
- [45] K. G. Klimenko. On Necessary and Sufficient Conditions for Some Higgs Potentials to Be Bounded From Below. *Theor. Math. Phys.*, 62:58–65, 1985.
- [46] Marc Sher. Electroweak Higgs Potentials and Vacuum Stability. *Phys. Rept.*, 179:273–418, 1989.
- [47] Shuquan Nie and Marc Sher. Vacuum stability bounds in the two Higgs doublet model. *Phys. Lett. B*, 449:89–92, 1999.
- [48] Shinya Kanemura, Takashi Kasai, and Yasuhiro Okada. Mass bounds of the lightest CP even Higgs boson in the two Higgs doublet model. *Phys. Lett. B*, 471:182–190, 1999.
- [49] Shinya Kanemura, Takashi Kasai, Guey-Lin Lin, Yasuhiro Okada, Jie-Jun Tseng, and C. P. Yuan. Phenomenology of Higgs bosons in the Zee model. *Phys. Rev. D*, 64:053007, 2001.
- [50] P. M. Ferreira, R. Santos, and A. Barroso. Stability of the tree-level vacuum in two Higgs doublet models against charge or CP spontaneous violation. *Phys. Lett. B*, 603:219–229, 2004. [Erratum: *Phys.Lett.B* 629, 114–114 (2005)].
- [51] Vernon Barger, Paul Langacker, Mathew McCaskey, Michael Ramsey-Musolf, and Gabe Shaughnessy. Complex Singlet Extension of the Standard Model. *Phys. Rev. D*, 79:015018, 2009.
- [52] I. F. Ginzburg, K. A. Kanishev, M. Krawczyk, and D. Sokolowska. Evolution of Universe to the present inert phase. *Phys. Rev. D*, 82:123533, 2010.
- [53] Kaori Fuyuto and Eibun Senaha. Improved sphaleron decoupling condition and the Higgs coupling constants in the real singlet-extended standard model. *Phys. Rev. D*, 90(1):015015, 2014.

- [54] C. Dohmen et al. Test of lepton flavor conservation in $\mu \rightarrow e$ conversion on titanium. *Phys. Lett. B*, 317:631–636, 1993.
- [55] Wilhelm H. Bertl et al. A Search for muon to electron conversion in muonic gold. *Eur. Phys. J. C*, 47:337–346, 2006.
- [56] Marcela Carena, Alejandro Daleo, Bogdan A. Dobrescu, and Timothy M. P. Tait. Z' gauge bosons at the Tevatron. *Phys. Rev. D*, 70:093009, 2004.
- [57] G. Cacciapaglia, C. Csaki, G. Marandella, and A. Strumia. The Minimal Set of Electroweak Precision Parameters. *Phys. Rev. D*, 74:033011, 2006.
- [58] Erik Lundstrom, Michael Gustafsson, and Joakim Edsjo. The Inert Doublet Model and LEP II Limits. *Phys. Rev. D*, 79:035013, 2009.
- [59] Tania Robens and Tim Stefaniak. Status of the Higgs Singlet Extension of the Standard Model after LHC Run 1. *Eur. Phys. J. C*, 75:104, 2015.
- [60] Grace Dupuis. Collider Constraints and Prospects of a Scalar Singlet Extension to Higgs Portal Dark Matter. *JHEP*, 07:008, 2016.
- [61] Michael E. Peskin and Tatsu Takeuchi. A New constraint on a strongly interacting Higgs sector. *Phys. Rev. Lett.*, 65:964–967, 1990.
- [62] Michael E. Peskin and Tatsu Takeuchi. Estimation of oblique electroweak corrections. *Phys. Rev. D*, 46:381–409, 1992.
- [63] D. Toussaint. Renormalization Effects From Superheavy Higgs Particles. *Phys. Rev. D*, 18:1626, 1978.
- [64] Vernon Barger, Paul Langacker, Mathew McCaskey, Michael J. Ramsey-Musolf, and Gabe Shaughnessy. LHC Phenomenology of an Extended Standard Model with a Real Scalar Singlet. *Phys. Rev. D*, 77:035005, 2008.
- [65] Shinya Kanemura, Yasuhiro Okada, Hiroyuki Taniguchi, and Koji Tsumura. Indirect bounds on heavy scalar masses of the two-Higgs-doublet model in light of recent Higgs boson searches. *Phys. Lett. B*, 704:303–307, 2011.
- [66] Ernesto Arganda and Maria J. Herrero. Testing supersymmetry with lepton flavor violating tau and mu decays. *Phys. Rev. D*, 73:055003, 2006.
- [67] Amon Ilakovac, Apostolos Pilaftsis, and Luka Popov. Charged lepton flavor violation in supersymmetric low-scale seesaw models. *Phys. Rev. D*, 87(5):053014, 2013.
- [68] Takashi Toma and Avelino Vicente. Lepton Flavor Violation in the Scotogenic Model. *JHEP*, 01:160, 2014.
- [69] Marco Ardu and Gianantonio Pezzullo. Introduction to Charged Lepton Flavor Violation. *Universe*, 8(6):299, 2022.
- [70] A. M. Baldini et al. MEG Upgrade Proposal. 1 2013.
- [71] A. Blondel et al. Research Proposal for an Experiment to Search for the Decay $\mu \rightarrow eee$. 1 2013.
- [72] Paolo Gondolo and Graciela Gelmini. Cosmic abundances of stable particles: Improved analysis. *Nucl. Phys. B*, 360:145–179, 1991.

- [73] Alexander Belyaev, Giacomo Cacciapaglia, Igor P. Ivanov, Felipe Rojas-Abatte, and Marc Thomas. Anatomy of the Inert Two Higgs Doublet Model in the light of the LHC and non-LHC Dark Matter Searches. *Phys. Rev. D*, 97(3):035011, 2018.
- [74] Laura Lopez Honorez, Emmanuel Nezri, Josep F. Oliver, and Michel H. G. Tytgat. The Inert Doublet Model: An Archetype for Dark Matter. *JCAP*, 02:028, 2007.
- [75] Amit Dutta Banik and Debasish Majumdar. Inert doublet dark matter with an additional scalar singlet and 125 GeV Higgs boson. *Eur. Phys. J. C*, 74(11):3142, 2014.
- [76] Mohammed Omer Khojali, Ammar Abdalgabar, Amine Ahriche, and Alan S. Cornell. Dark matter in a singlet-extended inert Higgs-doublet model. *Phys. Rev. D*, 106(9):095039, 2022.
- [77] G. Alguero, G. Belanger, F. Boudjema, S. Chakraborti, A. Goudelis, S. Kraml, A. Mjallal, and A. Pukhov. micrOMEGAs 6.0: N-component dark matter. *Comput. Phys. Commun.*, 299:109133, 2024.
- [78] Jisuke Kubo, Ernest Ma, and Daijiro Suematsu. Cold Dark Matter, Radiative Neutrino Mass, $\mu \rightarrow e\gamma$, and Neutrinoless Double Beta Decay. *Phys. Lett. B*, 642:18–23, 2006.
- [79] Eugenio Del Nobile. The Theory of Direct Dark Matter Detection: A Guide to Computations. *Lect. Notes Phys.* 996 (2022), 4 2021.
- [80] Mayumi Aoki, Shinya Kanemura, and Hiroshi Yokoya. Reconstruction of Inert Doublet Scalars at the International Linear Collider. *Phys. Lett. B*, 725:302–309, 2013.
- [81] Shinya Kanemura, Mariko Kikuchi, and Kodai Sakurai. Testing the dark matter scenario in the inert doublet model by future precision measurements of the Higgs boson couplings. *Phys. Rev. D*, 94(11):115011, 2016.
- [82] Tomohiro Abe and Ryosuke Sato. Quantum corrections to the spin-independent cross section of the inert doublet dark matter. *JHEP*, 03:109, 2015.
- [83] S. Moretti. Pair production of charged Higgs scalars from electroweak gauge boson fusion. *J. Phys. G*, 28:2567–2582, 2002.
- [84] Alexandre Alves and Tilman Plehn. Charged Higgs boson pairs at the CERN LHC. *Phys. Rev. D*, 71:115014, 2005.
- [85] Jan Kalinowski, Wojciech Kotlarski, Tania Robens, Dorota Sokolowska, and Aleksander Filip Zarnecki. Benchmarking the Inert Doublet Model for e^+e^- colliders. *JHEP*, 12:081, 2018.
- [86] Shinya Kanemura, Michihisa Takeuchi, and Kei Yagyu. Probing double-aligned two-Higgs-doublet models at the LHC. *Phys. Rev. D*, 105(11):115001, 2022.
- [87] Lorenzo Basso, Alexander Belyaev, Stefano Moretti, and Giovanni Marco Pruna. Probing the Z-prime sector of the minimal B-L model at future Linear Colliders in the $e^+e^- \rightarrow \mu^+\mu^-$ process. *JHEP*, 10:006, 2009.
- [88] Scott Haselschwardt. Status of the lux-seplon dark matter experiment. <https://indico.uchicago.edu/event/427/contributions/1325/>, 8 2024.